Translational Oncology 15 (2022) 101260

Contents lists available at ScienceDirect

Translational Oncology

journal homepage: www.elsevier.com/locate/tranon

A novel strategy for combination of clofarabine and pictilisib is synergistic in gastric cancer

Shayan Khalafi [a], Shoumin Zhu [a,b], Rimpi Khurana [c], Ines Lohse [d,e,f], Silvia Giordano [g,h], Simona Corso [g,h], Hassan Al-Ali [b,i,j,k,l], Shaun P. Brothers [d,e], Claes Wahlestedt [d,e], Stephan Schürer [b,c,m], Wael El-Rifai [a,b,n,*]

[a] Department of Surgery, Miller School of Medicine, University of Miami, Rosenstiel Medical Science Bldg, 1600 NW 10th Ave, Room 4007, Miami, FL 33136-1015, United States
[b] Sylvester Comprehensive Cancer Center, Miller School of Medicine, University of Miami, Miami, FL 33136, United States
[c] Department of Pharmacology, Miller School of Medicine, University of Miami, Miami, FL 33136, United States
[d] Center for Therapeutic Innovation, Miller School of Medicine, University of Miami, Miami, FL 33136, United States
[e] Department of Psychiatry and Behavioral Sciences, Miller School of Medicine, University of Miami, Miami, FL 33136, United States
[f] Molecular Therapeutics Shared Resource, Sylvester Comprehensive Cancer Center, University of Miami, FL 33136, United States
[g] Department of Oncology, University of Torino, Candiolo 10060, Italy
[h] Candiolo Cancer Institute, FPO-IRCCS, Candiolo 10060, Italy
[i] Department of Neurological Surgery, Miller School of Medicine, University of Miami, Miami, FL 33136, United States
[j] Department of Medicine, Miller School of Medicine, University of Miami, Miami, FL 33136, United States
[k] Peggy and Harold Katz Drug Discovery Center, Miller School of Medicine, University of Miami, Miami, FL 33136, United States
[l] The Miami Project to Cure Paralysis, Miller School of Medicine, University of Miami, Miami, FL 33136, United States
[m] Institute for Data Science and Computing, University of Miami, Miami, FL 33136, United States
[n] Department of Veterans Affairs, Miami Healthcare System, Miami, FL 33136, United States

ARTICLE INFO

Keywords:
Clofarabine
Pictilisib
Gastric cancer
Drug synergy
Combination therapy

ABSTRACT

Gastric cancer (GC) is frequently characterized by resistance to standard chemotherapeutic regimens and poor clinical outcomes. We aimed to identify a novel therapeutic approach using drug sensitivity testing (DST) and our computational SynerySeq pipeline. DST of GC cell lines was performed with a library of 215 Federal Drug Administration (FDA) approved compounds and identified clofarabine as a potential therapeutic agent. RNA-sequencing (RNAseq) of clofarabine treated GC cells was analyzed according to our SynergySeq pipeline and identified pictilisib as a potential synergistic agent. Clonogenic survival and Annexin V assays demonstrated increased cell death with clofarabine and pictilisib combination treatment ($P<0.01$). The combination induced

Abbreviations: GC, Gastric Cancer; DST, Drug sensitivity testing; FDA, Federal Drug Administration; DSB, Double strand breaks; RNAseq, RNA sequencing; H2AX, H2A histone family member X; AKT, Protein Kinase B; qRT-PCR, Quantitative real time polymerase chain reaction; BLC2, B-cell lymphoma 2; PDX, Patient derived xenograft; LINCS, Library of integrated network-based cellular signatures; TCGA, The cancer genome atlas; GBM, Glioblastoma multiforme; CIB, Clofarabine; ALL, Acute lymphoblastic leukemia; PI3K, Phosphoinositide 3-kinase; mTOR, Mechanistic target of rapamycin; PICT, Pictilisib; CHK2, Checkpoint kinase 2; PARP, Poly ADP-ribose polymerase; RPS6KB1, ribosomal protein S6 kinase beta-1; ATCC, American type cell culture collection; FBS, Fetal bovine serum; P/S, Penicillin/streptomycin; RPMI, Roswell Park memorial institute; STR, Short tandem repeat; NCI DTP, National Cancer institute drug testing program; STAR, Spliced transcripts alignment to a reference; GO, Gene ontology; DEG, Differentially expressed genes; KEGG, Kyoto encyclopedia of genes and genomes; STAD, Stomach adenocarcinoma; FDR, False discovery rate; PBS, Phosphate buffered saline; CI, Combination index; RIPA, Radioimmunoprecipitation assay; RPM, Rotations per minute; SDS-PAGE, sodium dodecyl sulfate–polyacrylamide gel electrophoresis; PVDF, Polyvinylidene difluoride; HRP, Horseradish peroxidase; cDNA, complementary DNA; HPRT, Hypoxanthine-guanine phosphoribosyltransferase; DAPI, 4′,6-diamidino-2-phenylindole; EDTA, Ethylenediaminetetraacetic acid; IP, Intraperitoneal; DMSO, Dimethylsulfoxide; OG, Oral gavage; ANOVA, Analysis of variance; DSSmod, Modified drug sensitivity score; sDSSmod, Selective modified drug sensitivity score; 5-FU, 5-fluorouracil; RR, Ribonucleotide reductase; HDAC, Histone deacetylase; ER, Estrogen receptor; PCA, Principle component analysis; DR, Discordance ratio; IC50, 50% inhibitory concentration; FITC, Fluorescein isothiocyanate; PI, Prodidium iodide; BAX, BCL2-associated X; BAD, BCL2-associated agonist of cell death; PUMA, p53 upregulated modulator of apoptosis; HER2, Human epidermal growth factor receptor 2; EBV, Epstein-Barr virus; PTEN, Phosphatase and tensin homolog; EMT, Epithelial-mesenchymal transition; AML, Acute myeloid leukemia.

* Corresponding author at: Department of Surgery, Miller School of Medicine, University of Miami, Rosenstiel Medical Science Bldg, 1600 NW 10th Ave, Room 4007, Miami, FL 33136-1015, United States.
E-mail address: welrifai@med.miami.edu (W. El-Rifai).

https://doi.org/10.1016/j.tranon.2021.101260
Received 17 July 2021; Received in revised form 8 October 2021; Accepted 25 October 2021
Available online 1 November 2021

double strand breaks (DSB) as indicated by phosphorylated H2A histone family member X (γH2AX) immunofluorescence and western blot analysis ($P<0.01$). Pictilisib treatment inhibited the protein kinase B (AKT) cell survival pathway and promoted a pro-apoptotic phenotype as evidenced by quantitative real time polymerase chain reaction (qRT-PCR) analysis of the B-cell lymphoma 2 (BCL2) protein family members ($P<0.01$). Patient derived xenograft (PDX) data confirmed that the combination is more effective in abrogating tumor growth with prolonged survival than single-agent treatment ($P<0.01$). The novel combination of clofarabine and pictilisib in GC promotes DNA damage and inhibits key cell survival pathways to induce cell death beyond single-agent treatment.

Introduction

Although the incidence of GC has declined over the past few decades, it remains the third leading cause of cancer-associated death worldwide, causing more than 700,000 deaths each year [1,2]. In the United States, 27,600 new cases of GC will be diagnosed in 2020, with an estimated 11,010 deaths [3]. Unfortunately, most patients with GC are initially asymptomatic and are diagnosed with late-stage disease once symptoms develop. Approximately 50% of patients will have tumors extending beyond locoregional confines at the time of diagnosis. Only half of those patients with localized tumors and will have tumors amenable to potentially curative resection [4]. The primary treatment option for patients with unresectable disease remains chemotherapy. Unfortunately, these therapies only achieve modest results and are often met with resistance and therapeutic failure [5]. Thus, there remains a significant need to discover novel therapeutic strategies in the treatment of GC.

Precision medicine approaches using DST have grown in popularity as a part of institutional personalized medicine initiatives. Our DST platform has been previously used in hematologic and solid tumors for drug sensitivity profiling of *ex-vivo* tumor samples [6–8]. Additionally, we have previously developed a computation platform, SynergySeq, to identify compounds that can be used in synergistic combination with a reference compound [9]. The platform utilizes the L1000 transcriptional-response profiles generated by the library of integrated network-based cellular signatures (LINCS) project. It creates perturbation-specific transcriptional signatures integrated with disease-specific profiles derived from The Cancer Genome Atlas (TCGA) transcriptional data. SynergySeq has been used to identify patient-specific drug combinations in glioblastoma multiforme (GBM) [10].

Clofarabine (CIB) is a next generation deoxyadenosine analogue derived from cladribine and fludarabine. It was rationally designed such that its deoxyadenosine analog structure inhibits DNA synthesis at two critical junctures: DNA polymerase I and RNA reductase [11]. This results in significant DNA damage and DSB, ultimately culminating in apoptosis [12]. The FDA granted approval in 2004 for the use of clofarabine monotherapy for pediatric patients with relapsed or refractory acute lymphoblastic leukemia (ALL) [13]. While most investigations have evaluated its effect in hematological malignancies, there is growing preclinical evidence that clofarabine may have efficacy in solid tumors as well, especially colorectal cancer [14,15]. However, the efficacy of clofarabine in solid tumors remains largely undetermined.

The AKT/phosphoinositide 3-kinase (PI3K)/mechanistic target of rapamycin (mTOR) pathway has been shown to be constitutively activated in approximately 80% of human gastric adenocarcinoma samples [16]. Moreover, alterations in this signaling pathway play an important role in chemoresistance of various standard chemotherapeutic regimens [17]. Pictilisib (PICT) is an orally bioavailable inhibitor of PI3K that had a clinical effect in various solid tumors [18,19]. Owing to the prevalence of PI3K pathway alterations in chemoresistance, pictilisib has been investigated in phase I clinical trials as a combination treatment with standard chemotherapy in various solid tumors [20,21].

In this study, we use DST screening to select a list of agents from a library of 215 FDA approved anti-cancer compounds available on compassionate care. This library consists of agents covering a variety of targets and pathways relevant to GC. Our screening identified clofarabine as a potential therapeutic agent. We then performed next generation sequencing of GC cells treated with clofarabine and analyzed the transcriptional expression pattern to identify a second agent that would function synergistically to achieve maximum antitumor effect. Utilizing this SenergySeq pipeline, we found that treatment with clofarabine resulted in a robust antitumor activity that was enhanced with the cotreatment of pictilisib *in vitro* and *in vivo*.

Materials and methods

Antibodies and reagents

Clofarabine (S1218) was obtained from Selleck Chemicals (Houston, TX) and Pictilisib (HY-50094) was obtained from MedChemExpress (Monmouth Junction, NJ). AKT (4691), p-AKT (4060), checkpoint kinase 2 (CHK2) (6334), p-CHK2(2197), H2AX (7631), p-H2AX (9718), poly ADP-ribose polymerase (PARP) (9542), cleaved PARP (5625), ribosomal protein S6 kinase beta-1 (RPS6KB1) (9202), p-RPS6KB1 (9205), BCL2 (15071), BCL2-associated X (BAX) (5023), p53 upregulated modulator of apoptosis (PUMA) (98672), and cleaved caspase 3 (9661) antibodies were all obtained from Cell Signal Technology (Danvers, MA). Ki67 (27309) antibody was obtained from Proteintech (Rosemont, IL). β-Actin antibody was obtained from Millipore Sigma (St. Louis, MO).

Cell culture

The gastric adenocarcinoma cell lines AGS, SNU1, MKN28, MKN45, and STKM2 were used in the study. The immortalized nonneoplastic gastric (GES1) and esophageal (EPC2) cell lines were included as normal controls. AGS and SNU1 cells were purchased from American Type Culture Collection (ATCC, Manassas, VA). MKN28 and MKN45 cells were obtained from the Riken Cell Bank (Tsukuba, Japan). EPC2 cells were kindly provided by Dr. Anil Rustgi (University of Pennsylvania, Philadelphia, PA). GES1 cells were kindly provided by Dr. Dawit Kidane-Mulat (University of Texas at Austin, Austin, TX). AGS cells were cultured in Ham's F12 media (GIBCO, Carlsbad, CA) supplemented with 5% fetal bovine serum (FBS, Invitrogen Life Technologies, Carlsbad, CA) and 1% penicillin/streptomycin (P/S) (GIBCO). MKN28, MKN45, and GES1 cells were cultured in Roswell Park memorial institute (RPMI) medium (GIBCO) supplemented with 10% FBS and 1% P/S. EPC2 cells were cultured in Keratinocyte serum-free medium supplemented with recombinant epidermal growth factor and bovine pituitary extract (GIBCO). All cell lines were ascertained to conform to the original *in vitro* morphological characteristics and were authenticated using short tandem repeat (STR) profiling (Genetica DNA Laboratories, Burlington, NC). All cell lines reported here have been tested and had shown to be free of mycoplasma (R&D Systems, Minneapolis, MN).

DST screening

A range of FDA approved anti-cancer compounds ($n = 215$) were utilized in a compound library covering various targets and pathways

relevant to gastric adenocarcinoma. The compounds were obtained from the National Cancer Institute Drug Testing Program (NCI DTP) and commercial vendors (Enzo Life Sciences, Selleck Chemicals, Sigma-Aldrich, Tocris Biosciences). Drug sensitivity testing was performed as described previously [6–8]. All compounds were dissolved in 100% dimethyl sulfoxide (DMSO) and tested in duplicate using a 10-point 1:3 dilution series starting at a nominal test concentration of 10 μM (20, 000-fold concentration range). One thousand cells from the AGS, MKN28 and EPC2 cell lines were seeded per well in 384-well micro-titer plates and incubated in the presence of compounds in a humidified environment at 37 °C and 5% CO_2. After 72 h of treatment, cell viability was assessed by measuring ATP levels via bioluminescence (CellTiter--Glo; Promega, Madison, WI, USA) and dose–response curves were generated for each compound. Interpretation of curve parameters was performed according to the modified drug-sensitivity scoring (DSSmod) function we previously developed [6]. As a final step, the selective DSSmod (sDSSmod) for each drug in each patient screen was calculated according to the formula: sDSSmod=DSSmod (cancer cells) − DSSmod (normal cells).

mRNA sequencing

AGS and MKN45 cells were seeded in a 6-well plate at a density of 2 × 10^5 cells per well. Cells were treated with clofarabine (200 nmol/L) for 48 h. According to the manufacturer's specifications, RNA was isolated using the RNeasy Mini Kit (Qiagen, Valencia, CA). mRNA sequencing was performed by Novogene corporation (Sacramento, CA). RNA purity was assessed using the NanoPhotometer spectrophotometer (IMPLEN, CA). RNA integrity and quantitation were assessed using the RNA Nano 6000 Assay Kit of the Bioanalyzer 2100 system (Agilent Technologies, CA). A total of 1 μg RNA per sample was used as input material for the RNA sample preparations. According to the manufacterer's instructions, the clustering of the index-coded samples was performed on an Illumina Novaseq 6000 sequencer (Illumina Inc, CA, USA). After cluster generation, the libraries were sequenced on the same machine and paired-end reads were generated. A sequencing depth of 20 million paired-end 150 base pair reads was performed. The initial quality control services were performed by Novogene of data generated from the Illumina Novaseq 6000 sequencer.

RNA sequencing analysis

Following mRNA sequencing, the sequencing reads were aligned to the human reference genome using spliced transcripts alignment to a reference (STAR) [22]. The raw read count matrix was then analyzed using the DESeq2 R package to compute the gene expression levels between the clofarabine treated cell lines and untreated cell lines [23]. Genes with $\log_2FC > 1$ with an adjusted P value < 0.05 were considered differentially expressed.

Gene ontology (GO) enrichment analysis was performed on the differentially expressed genes (DEG) using R package cluster Profiler with org.Hs.eg.db used for annotation [24,25]. Enriched GO pathways with an adjusted P value < 0.05 were identified after the Benjamini-Hochberg correction for multiple testing [26]. Signaling pathways were identified using the Kyoto Encyclopedia of Genes and Genomes (KEGG) [27].

Data from various databases was processed, including the RNA sequencing data from the TCGA and L1000 datasets [28]. The TCGA data from stomach adenocarcinoma (STAD) comprised of 415 patients with tumors and 37 health controls and was downloaded from recount2 [29]. The data was pre-processed using our previously described pipeline [9]. We then used the R package TCGAbiolinks to compare the raw counts [30]. Differential expression analysis was performed on the filtered genes and genes with $\log_2FC > 1$. The false discovery rate (FDR) threshold of 0.01 was considered significantly differentially expressed. We then performed a similar analysis on the L1000 dataset downloaded from the Broad Institute's LINCS data portal (http://lincsportal.ccs.miami.edu/). This dataset consists of 978 landmark transcripts. Gene expression data were combined, and compound annotations were unified for further data analysis.

SynergySeq analysis

We applied our previously described SynergySeq pipeline [10] to identify compounds synergistic with clofarabine. As descrobed above, we first identified the DEG in clofarabine treated and untreated GC cell lines (AGS and MKN45). We then utilized the L1000 dataset to define the transcriptional signature of the compounds included in this dataset. The L1000 repository contains gene expression profiles for thousands of small molecules and drugs. The overlap between the transcriptional signatures of L1000 compounds and the DEG from GC cell lines treated with clofarabine was used to define the individual drug signatures. These L1000 compound drug signatures were ranked according to their similarity to the transcriptional signature of clofarabine treated cells. We then investigated the TCGA STAD tumor samples and same tissue controls to identify differentially expressed genes which we defined as the disease signature expression profile. Next, the disease signatures were computed to identify the L1000 molecules that reverse these reverse the STAD disease signature. Finally, an orthogonality score was computed for L1000 compounds based on their similarity to the clofarabine reference signature and reversal of the STAD reference disease signature.

Clonogenic survival assay

AGS and MKN45 cells were rinsed with PBS, trypsinized, and collected as a single cell suspension. Cells were seeded in a 6 well plate at a density of 1000 cells per plate. Cells were allowed to attach overnight. The following day, the cells were treated with clofarabine (100 or 200 nmol/L) and pictilisib (0.5 or 1 μmol/L), as a single agent or in combination or with vehicle control. After 48 h of treatment, media was replaced with regular drug-free media. After incubation for 10 days, colonies were fixed using 4% paraformaldehyde. Colonies were then stained using 0.05% crystal violet. Colonies were counted using ImageJ (https://imagej.nih.gov/ij/index.html) and the ColonyArea plugin (https://b2share.eudat.eu/records/39fa39965b314f658e4a198a78d7f6b5).

Cell viability assay

Cells were rinsed with PBS, trypsinized, and collected as a single cell suspension. Cells were seeded in a 96 well microplate at a density of 1000 cells per well with 2% FBS media. Cells were treated with clofarabine (0–4 μmol/L) and pictilisib (0–16 μmol/L), as a single agent or in combination or with vehicle control. After 96 h of treatment, the CellTiter-Glo Cell Viability Assay (Promega, Madison, WI, USA) reagent was added to the sample. According to the manufacturer's instructions, luminescence was measured using the FLUOROstar Optima (BMG Labtech, Ortenberg, Germany).

Synergism analyses

Compound synergy was quantified using the Chou-Talalay method and the CompuSyn software (https://www.combosyn.com/). First, the dose-effect curve for each drug alone is determined using the median-effect principle. It is compared with the effect achieved with a combination of the two drugs to derive a combination index (CI) value. The CI indicates the level of synergism or antagonism observed between two drugs: <0.9 indicates synergism (0.3–0.7 strong; 0.7–0.85 moderates; 0.85–0.9 slight), 0.9–1.1 indicates an additive effect, and >1.1 indicates antagonism [31].

Western blotting

Cells were plated at a density of density of 2×10^5 cells per well and treated with clofarabine (500 nmol/L), pictilisib (2 μmol/L) or a combination of both agents for 6, 24, or 48 h. Following treatment, cells were lysed by sonication in a radioimmunoprecipitation assay (RIPA) protein lysis buffer (Santa Cruz Biotechnology, Dallas, TX). Cellular proteins were collected in the supernatant fraction following centrifugation at 13,000 rotations per minute (RPM) for 10 min at 4 °C. Proteins were separated on 10% or 12.5% sodium dodecyl sulfate–polyacrylamide gel electrophoresis (SDS-PAGE) and transferred to Immobilon polyvinylidene difluoride (PVDF) membranes (Millipore Sigma). Membranes were probed with specific antibodies, and proteins were visualized using horseradish peroxidase (HRP)-conjugated secondary antibodies and Immobilon Western Chemiluminescent HRP Substrate detection reagent (Millipore Sigma). Gel loading was normalized for equal detection of the β-actin signal. All immunoblots were imaged using the Biorad ChemiDoc XRS+ system (Bio-Rad, Hercules, CA).

qRT-PCR

AGS and MKN45 cells were seeded in a 6-well plate at a density of 2×10^5 cells per well. Cells were treated with clofarabine (500 nmol/L), pictilisib (2 μmol/L) or a combination of both agents for 24 h. RNA was isolated using the RNeasy Mini Kit (Qiagen). Single-stranded complementary DNA (cDNA) was synthesized using the High-Capacity cDNA Reverse Transcription Kit (Applied Biosystems, Waltham, MA). Genes specific for human primers were designed using the online software Primer 3 (https://primer3.ut.ee/). Forward and reverse primers were designed to span two different exons for each tested gene. The primer sequences can be found in supplemental Table 1. All primers were purchased from Integrated DNA Technologies (Coralville, IA). qRT-PCR was performed using the CFX96 Real-Time PCR detection system (Bio-Rad). The threshold cycle number was determined according to the iCycler Software version 3.1. Reactions were performed in duplicate, and the threshold cycle numbers were averaged. Threshold values were normalized to the housekeeping gene Hypoxanthine-guanine phosphoribosyltransferase (HPRT). Expression ratios were calculated with the $\Delta\Delta C_t$ method [32].

Immunofluorescence

AGS and MKN45 cells were seeded in an 8-well cell culture chamber slide at a density of 1×10^4 cells per well. Cells were treated for 48 h with clofarabine (0.5 μmol/L) and pictilisib (2 μmol/L) as a single agent or in combination or with vehicle control. Cells were then fixed with freshly prepared 4% paraformaldehyde in PBS solution for 45 min at room temperature. A permeabilization solution of 0.1% Triton X-100 (Millipore Sigma) in 0.1% sodium citrate (Millipore Sigma) was then added for 5 min on ice. The cells were then blocked for 1 hour using 10% normal goat serum (Thermo Fisher Scientific, Waltham, MA). The cells were then incubated with an anti-γ-H2AX antibody overnight at 4 °C. A secondary antibody of Alex Fluor 568 goat anti-rabbit IgG (Thermo Fisher Scientific) was added, and coverslips were mounted with VECTASHIELD Mounting Medium containing 4′,6-diamidino-2-phenylindole (DAPI) counterstain cellular nuclei. γ-H2AX foci were scored manually using an Olympus fluorescence microscope. The number of cells with positively staining foci was calculated from a minimum of 250 cells per treatment condition. Experimental data represents the average of three independent experiments.

Immunohistochemistry

Ki67 and cleaved caspase 3 immunohistochemical analysis was performed on formalin-fixed, paraffin-embedded tissues. Tissue sections were deparaffinized and antigen retrieval was carried out using either Tris-ethylenediaminetetraacetic acid (EDTA) (pH 9.0) or sodium citrate (pH 6.0) buffer based on primary antibody manufacturer recommendations. The Millipore IHC Select (Millipore Sigma) immunoperoxidase secondary detection system was utilized according to manufacturer instructions. Diaminobenzidine staining signal was quantified using ImageJ FIJI as previously described [33].

14 in vivo experiments

Five-week-old NOD.Cg-Prkdc^{scid}/J mice were purchased from Jackson Laboratory (Bar Harbor, ME). De-identified PDXs from human gastric adenocarcinoma were generated according to our previously described platform [34]. PDX lines 498 and 459 were used in the experiment. Both PDX lines were generated from patients with advanced (stage IV) disease and histologically were the intestinal subtype based on Lauren classification (Supplemental Table 2). Samples were cut to a uniform size and implanted subcutaneously into bilateral flanks. Tumors were measured every other day until tumor volume reached approximately 150 mm^3. The mice were then randomized into 4 groups containing 9 mice and treated with clofarabine, pictilisib, or a combination for 24 days. Clofarabine was delivered via intraperitoneal (IP) injection at a dose of 30 mg/kg every 3 days. The IP formulation consisted of 4% DMSO in PBS + 1% Tween-80. Pictilisib was delivered via oral gavage (OG) at a dose of 75 mg/kg administered according to the schedule 5 days on, 2 days off. The OG formulation consisted of 0.5% methylcellulose in PBS + 0.2% Tween-80. Tumor growth was determined by measuring the width and length of the tumors with an electronic caliper every 3 days. Body weights were measured every 7 days to monitor for drug toxicity. Tumor volume was calculated using the following formula: tumor volume (mm^3) = $1/2\ (W)^2$ x (L). At the experimental treatment endpoint of 24 days, 6 mice from each group were followed for survival. These mice were sacrificed once tumors reached 1000 mm^3. A Kaplan-Meier survival estimate was performed with a log-rank calculation to determine statistical significance. All *in vivo* experiments were approved by the University of Miami's Institutional Animal Care and Use Committee and performed according to all guidelines (protocol number 20–110).

Statistical analysis

Values were expressed as a mean +/- standard deviation. All *in vitro* experiments were the results of at least three independent experiments. GraphPad Prism 8 (GraphPad Software Inc., CA) software was used for all statistical analyses. One-way analysis of variance (ANOVA) with TuKey post-hoc analysis was utilized to demonstrate statistical differences between control groups and treatment groups. The P value of ≤ 0.05 were considered statistically significant and are marked in the figures: * represents $P < 0.05$, ** represents $P < 0.01$.

Results

Drug sensitivity profiling of GC cell lines identifies clofarabine an efficacious agent in vitro

Neoplastic (AGS, MKN28) and normal (EPC2) gastroesophageal epithelial cell lines were exposed to a library containing 215 FDA-approved anti-cancer compounds. The modified drug sensitivity score (DSSmod) method has been described previously [6–8]. Briefly, The DSSmod represents a score of the compound's anti-proliferative/cytotoxic activity that incorporates both potency and efficacy measures. The selective DSSmod (sDSSmod) was determined by calculating the difference in DSSmod between cancer cell lines and the normal EPC2 cell line. sDSSmod reveals therapies with the greatest tumor-selective activity (higher activity against cancer cells relative to normal non-cancer cells). Consequently, sDSSmod serves to deprioritize

treatments that exhibit high toxicity towards normal tissue and prioritize treatments with high selective activity towards tumor tissue. Compounds with sDSSmod $\geq$ 5 were prioritized and ranked by their sDSSmod score. 54 and 41 compounds displayed responses above threshold in AGS and MKN28 cells, respectively (Supplemental Fig. S1A, B). AGS and MKN28 cell lines demonstrated similar drug sensitivity to most active compounds (Fig. 1A); however, the ranking of specific hits differed between cell lines (Supplemental Fig. S1A,B). A significant response (DSSmod $\geq$ 5) was observed in 29 compounds tested in EPC2 cells, which serve as a normal tissue control (Supplemental Fig. S1C).

Current standard chemotherapeutic regimens for GC often include a DNA damaging drug. Agents that are commonly used include cisplatin, oxaliplatin, and 5-fluorouracil (5-FU) [35]. Our drug sensitivity profiling identified several DNA damaging agents that were efficacious in GC cell lines (Fig. 1A). These drugs have distinct mechanisms of action, including DNA topoisomerase inhibitors, ribonucleotide reductase (RR) inhibitors, and folate antimetabolites. Of these agents, we elected to investigate clofarabine based on its unique ability to inhibit not only RR but also DNA polymerase I. This nucleoside analog also disrupts mitochondrial function and membrane integrity, resulting in the release of pre-apoptotic factors like cytochrome C, and apoptotic-inducing factors [12]. In fact, the unique biochemical modulation of clofarabine, when used with other established chemotherapeutic regimens, has made it an attractive target for investigators as a component of combination chemotherapy [36]. Our drug sensitivity profiling of clofarabine demonstrated good anti-tumor activity in both AGS and MKN28 cell lines with minimal effect in the EPC2 cell line (Supplemental Fig. 1D–F). Thus, clofarabine was identified as a promising compound for our investigation.

Synergy-seq pipeline analysis to identify compounds with potentially synergistic activity with clofarabine

AGS and MKN45 cell lines were treated with clofarabine (0.3 μmol/L) for 48 h and total RNA was extracted for RNA sequencing. The RNA sequencing data was used to determine the differential expression levels in clofarabine treated GC cell lines and untreated samples. The dataset included 3 replicates from each group. Initially, clustering was performed on the raw expression dataset. By comparing the clofarabine treated GC cell lines to untreated control samples, we separated the drug treated samples from the untreated samples, as depicted by the principal component analysis (PCA) plot (Fig. 1B). In AGS cells, our analysis revealed 1882 genes with significant differences ($\log_2$FC>1 and P<0.05); 1490 genes were upregulated, and 392 genes were down-regulated in clofarabine treated cells compared to untreated samples (Fig. 1C) (Supplemental Table 2). In MKN45 cells, 1071 genes were found to be significantly differentially expressed with 901 upregulated and 170 down-regulated genes (Fig. 1D) (Supplemental Table 2). We performed the functional enrichment analysis on the DEG, including GO and KEGG pathway analyses. The top terms of GO functions were enriched in cell motility, migration, and differentiation. KEGG pathways were enriched for cytokine-cytokine receptor interaction and P53 signaling pathways (Supplemental Fig. 2A,B). Differential expression analysis of the TCGA RNAseq expression data identified 4982 DEG in gastric adenocarcinoma samples than healthy controls (Fig. 2A) (Supplemental Table 2).

We then attempted to evaluate the transcriptional difference between the clofarabine treated GC cell lines and the L1000 dataset. We identified 64 (AGS) and 35 (MKN45) genes out of a total of 978 L1000 genes that were shown to be differentially expressed in the clofarabine treated samples compared with untreated controls. The compounds with a low number of genes in the L1000 dataset were excluded. A concordance ratio was derived for each compound, describing the ratio of a compound's genes with similar regulation clofarabine to genes with the opposite regulation. This is represented as the orthogonality score compared to reference clofarabine treatment (Fig. 2B).

Next, we analyzed 168 significantly differentially expressed genes in the TCGA dataset that were present in the L1000 gene set. An optimal compound has the potential to reverse these 168 disease specific signatures. To determine suitable compounds, we computed the disease specific discordance ratio (DR) analogous to clofarabine (DEG in AGS and MKN45 cell lines) for all compounds. DR is used to describe the ratio of drug induced DEG that have opposite regulation to the disease signature (STAD) to those with the same regulation (Fig 2B). The L1000 compounds were ranked according to their concordance to the reference clofarabine signature in GC cell lines. To identify top agents suitable for potential synergism with clofarabine, we first ranked compounds based on their disease discordance ratio. The top 5 agents were selected from the list and then ranked according to orthogonality to reference clofarabine signature (Fig. 2B,C). A synergy plot was computed based on a compound's similarity to the reference clofarabine signature (x-axis) and the reversal of the disease signature (y-axis) (Supplemental Fig. 3A, B). Utilizing this pipeline, we were able to identify several candidate compounds with theoretical synergistic activity with clofarabine in GC cell lines.

Clofarabine and pictilisib demonstrate synergism in inhibiting GC cell viability

Utilizing the top results from the synergy pipeline; we next sought to validate the combinatorial effects of clofarabine with these agents. We performed the ATP-Glo cell viability assay in cells treated with clofarabine in combination with either NVP-TAE 684, simvastatin, foretinib, or pictilisib (Supplemental Fig. 4). We discovered that the combination of clofarabine and pictilisib performed better than others and substantially decreased cell viability in numerous cell models of GC (AGS, MKN45, SNU1), as compared with single agent treatments (Fig. 3A–C). We did not detect significant changes in cell viability of immortalized normal gastric epithelial cells (GES1) (Fig. 3D). Furthermore, we determined the CI utilizing the Chou-Talalay isobologram method [31]. Results demonstrated synergistic activity of combined clofarabine and pictilisib treatment in all tested GC cell lines (CI<0.7) (Fig. 3E).

For further validation, we performed a long-term (10 days) clonogenic survival assay. AGS and MKN45 cells were treated with clofarabine (0.1 μmol/L) and pictilisib (0.5 μmol/L) for 48 h. The results indicated a decrease in cell viability by 80% and 60% in AGS and MKN45 cells, respectively, with combined clofarabine and pictilisib treatment compared to vehicle control. This decrease in cell viability was significantly greater than single agent treatment with clofarabine (25%, 45%) or pictilisib (35%, 55%) (Supplemental Fig. S5A,B, P<0.01). Together, these results validate the synergistic activity of clofarabine and pictilisib in GC cell lines.

Combination treatment with clofarabine and pictilisib increases levels of DNA damage and induces cell death

Clofarabine mechanistically generates DSB that results in the induction of apoptosis [12]. An early cellular response to DSB is the phosphorylation of H2AX at the sites of DNA damage. Rapid phosphorylation at serine 139 results in discrete γ-H2AX foci at the DNA damage sites [37]. We analyzed the extent of DSB by performing immunofluorescent staining of γ-H2AX in AGS and MKN45 cells treated with clofarabine (0.5 μmol/L) and pictilisib (2 μmol/L) for 48 h. Cells treated with clofarabine alone had a significantly increased percentage of cells with DSB (AGS 31%, MKN45 25%) compared with vehicle control or pictilisib alone. When pictilisib was added in combination with clofarabine, DSB was significantly increased (AGS 68%, MKN45 54%) compared to all other treatment conditions, as demonstrated by positively staining γ-H2AX foci (Fig. 4A,B, $P < 0.01$).

The accumulation of DSB is a major cellular disturbance and culminates in apoptosis. To determine the degree to which treatment conditions resulted in apoptosis, we performed flow cytometry analysis

A

Drug Sensitivity Profiling in AGS and MKN28 Cells

Agent	AGS sDSSmod	MKN28 sDSSmod	Mechanism of Action
Belinostat	90.042	81.666	Pan-Histone deacetylase (HDAC) inhibitor
Topotecan	33.779	33.790	DNA topoisomerase I inhibitor
Methotrexate	36.615	30.766	Folate antimetabolite
Idarubicin	38.250	27.890	DNA topoisomerase II inhibitor
Camptothecin	29.571	30.677	DNA topoisomerase I inhibitor
Fludarabine	28.647	29.257	Ribonucleotide reductase (RR) inhibitor
Vincristine	26.685	26.658	Inhibitor of microtubule polymerization
Pemetrexed	28.321	24.029	Folate antimetabolite
Clofarabine	25.361	26.326	RR and DNA polymerase I inhibitor
Rapamycin	23.775	22.257	Specific mTOR inhibitor
Docetaxel	22.019	20.164	Inhibitor of microtubule depolymerization
Fulvestrant	21.474	19.786	Estrogen receptor (ER) antagonist

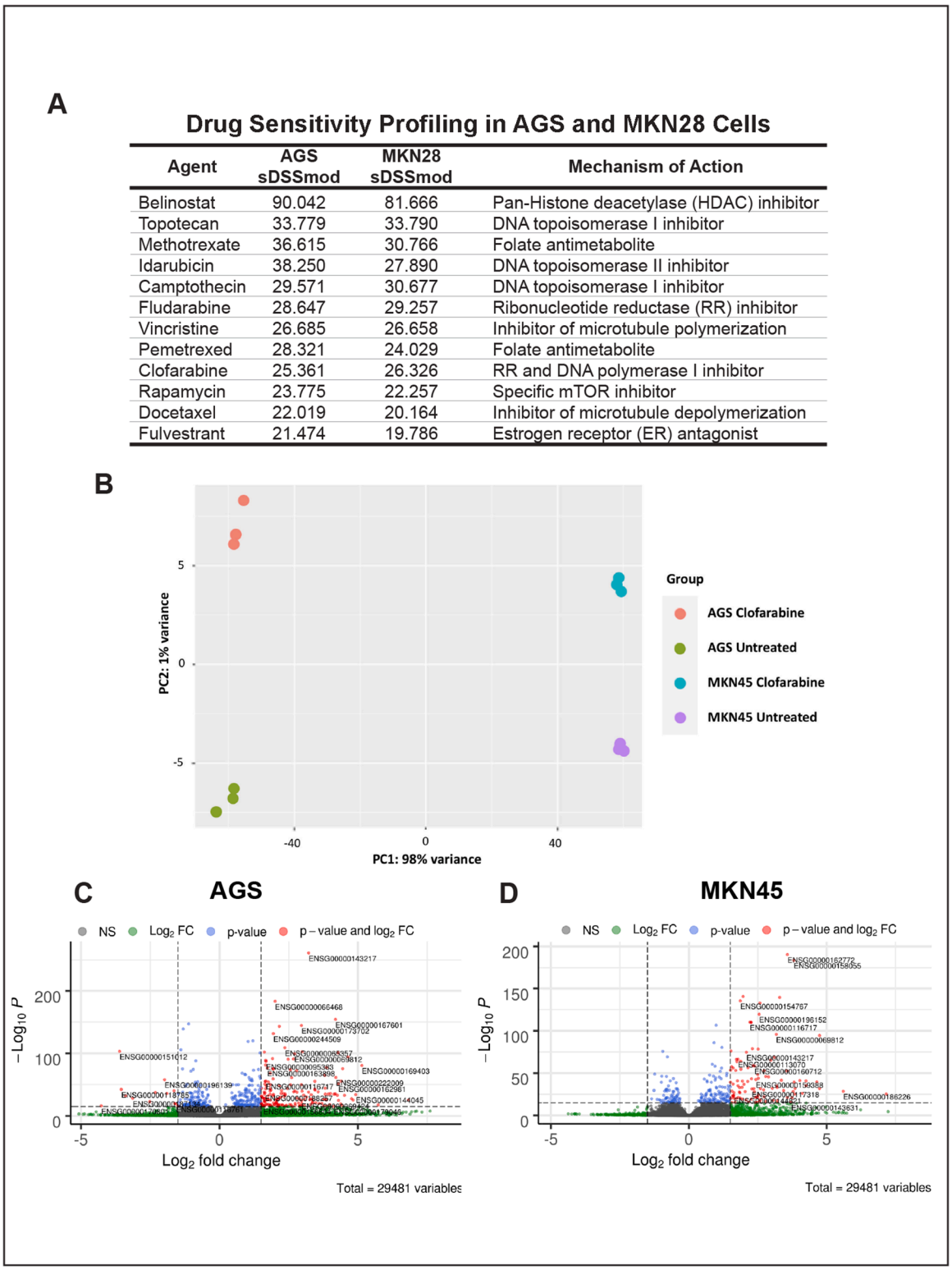

Fig. 1. Drug sensitivity profiling of GC cell lines and analysis of RNA sequencing signature of clofarabine treated GC cell lines. **A:** Table showing list of top agents with clinically actionable drug responses according to sDSSmod scoring in AGS and MKN28 cell lines. Displayed are agents that showed activity in both cell lines. Agents are ranked according to the average sDSSmod value in both cell lines. **B:** PCA plot showing AGS clofarabine treated samples (red, top left), AGS untreated samples (green, bottom left), MKN45 clofarabine treated samples (cyan, top right), and MKN45 untreated samples (purple, bottom right). The results represent 3 replicate samples for each treatment condition. **C-D:** Volcano plot showing differentially expressed genes between the clofarabine treated and untreated samples in AGS **(C)** and MKN45 **(D)** cell lines. Each dot is representative of a single gene. The vertical lines correspond to the $\log_2$ fold change of -1 and $+1$. The horizontal line indicates an adjusted P value of 0.05. The genes on the left are significantly downregulated and genes on the right are significantly upregulated.

A

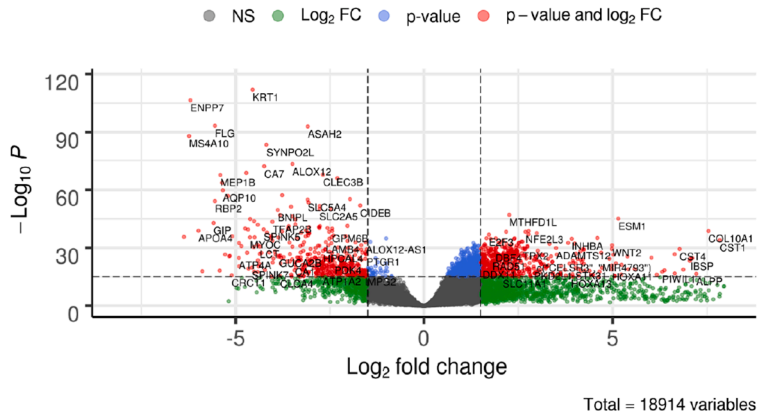

B

Candidate Compounds with Predicited Clofarabine Synergism

Agent	Disease Similar		Disease Opposite		Disease Discordance		Clofarabine Orthogonality	
	AGS	MKN45	AGS	MKN45	AGS	MKN45	AGS	MKN45
Pictilisib	0.053	0.050	0.816	0.775	0.408	0.388	0.067	0.014
NVP-TAE 684	0.026	0.025	1.000	1.000	1.000	1.000	0.037	0.034
Foretinib	0.053	0.050	0.947	0.900	0.474	0.450	0.120	0.022
Simvastatin	0.026	0.025	0.395	0.375	0.395	0.375	0.094	0.066
GSK-1070916	0.053	0.050	0.763	0.725	0.382	0.363	0.238	0.271

C

Agent	Mechanism of Action
Pictilisib	Selective PI3Kα/δ inhibitor
NVP-TAE 684	Selective ALK inhibitor
Foretinib	c-Met and VEGFR-2 inhibitor
Simvastatin	HMG-CoA reductase inhibitor
GSK-1070916	Aurora Kinase B/C competitive inhibitor

Fig. 2. Identification of candidate compounds with predicted synergism with clofarabine treatment. **A:** Volcano plot showing differentially expressed genes in the TCGA dataset between STAD samples and normal tissue controls. Each dot is representative of a single gene. The vertical lines correspond to the $\log_2$ fold change of −1 and +1. The horizontal line indicates an adjusted *P* value of 0.05. The genes on the left are significantly downregulated and genes on the right are significantly upregulated. **B:** Table listing the top 5 agents with predicted clofarabine synergism in AGS and MKN45 cell lines based on the SynergySeq pipeline. Compounds were first ranked based on disease discordance to DEG in STAD samples from the TCGA database. These compounds were then ranked according to orthogonality to reference clofarabine signature. **C:** Table depicting mechanism of action for candidate compounds with predicted synergism to clofarabine treatment.

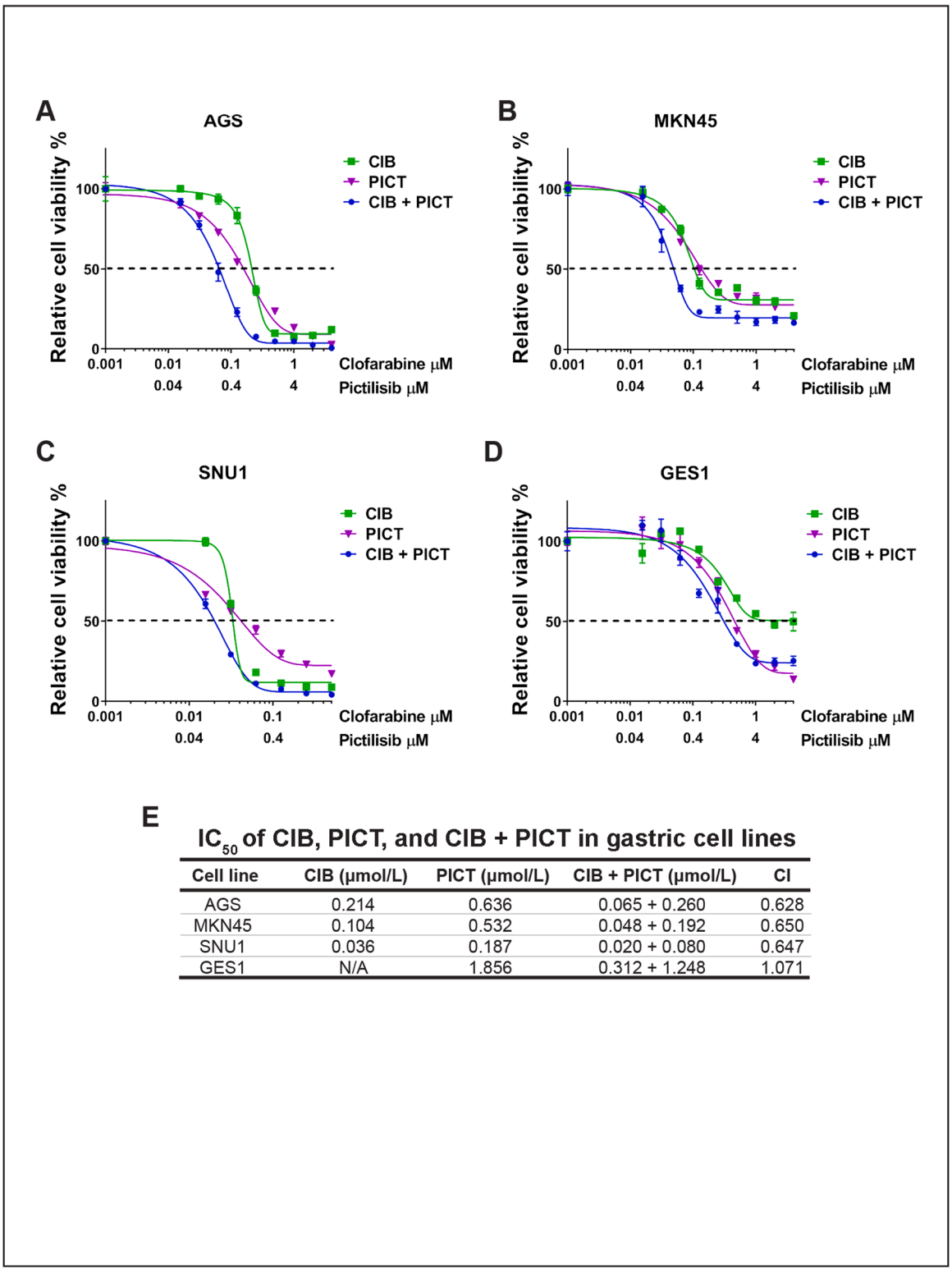

E

IC_{50} of CIB, PICT, and CIB + PICT in gastric cell lines

Cell line	CIB (μmol/L)	PICT (μmol/L)	CIB + PICT (μmol/L)	CI
AGS	0.214	0.636	0.065 + 0.260	0.628
MKN45	0.104	0.532	0.048 + 0.192	0.650
SNU1	0.036	0.187	0.020 + 0.080	0.647
GES1	N/A	1.856	0.312 + 1.248	1.071

Fig. 3. Clofarabine and pictilisib act synergistically in GC cell lines. **A–D:** ATP-Glo assay for clofarabine and pictilisib combination and single agent treatment for 72 h in GC cell lines (AGS, MKN45, SNU1) **(A-C)** and a normal, immortalized gastric epithelial cell line (GES1) **(D). E:** The summary of IC_{50} values of clofarabine, pictilisib, or clofarabine + pictilisib treatment of all malignant and normal gastric cell models. CI values display synergistic activity in the cell lines. CI was determined using the Chou-Talalay method for drug synergy.

with Annexin V-fluorescein isothiocyanate (FITC) and propidium iodide (PI) staining. Annexin V detects phosphatidylserine that is translocated from the inner to the outer leaflet of the plasma membrane in apoptotic cells. PI is a viability stain that is excluded from cells with intact plasma membranes. Taken together, cells staining positive for Annexin V and negative for PI are actively undergoing apoptosis, while cells staining positive for both markers are necrotic [38]. AGS and MKN45 cells were again treated with clofarabine (0.5 μmol/L) and pictilisib (2 μmol/L) for 48 h. We discovered a significantly increased population of apoptotic cells in both AGS and MKN45 cell lines when treated with clofarabine

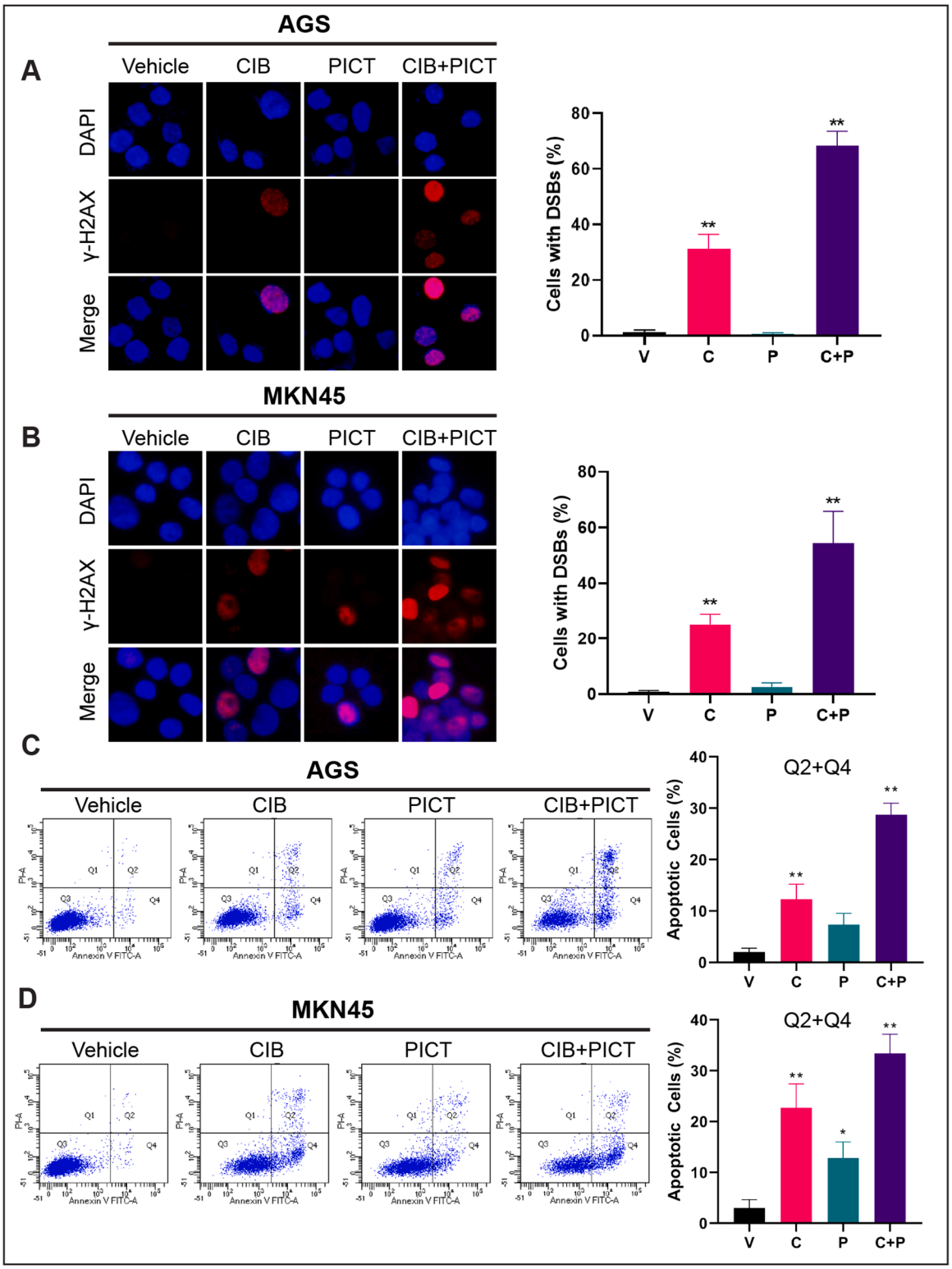

Fig. 4. Clofarabine and pictilisib in combination increase DNA damage and cell death. **A-B:** γ-H2AX (red) staining in AGS and MKN45 cells following clofarabine and/or pictilisib treatments (left) and relative percentage of cells with positively staining foci (right). **C-D:** The Annexin V-FITC and PI staining was performed following treatments in AGS and MKN45 cells. Bar graphs (right) represent the sum of Q2+Q4 events for each treatment condition. One-way ANOVA with Tu-Key post-hoc analysis was utilized to demonstrate statistical difference between control groups and treatment groups. Each bar in the graph to the right represents the mean ± SD of three independent experiments. * $P < 0.05$, ** $P < 0.01$.

and pictilisib in combination compared with single agent or vehicle controls (Fig. 4C,D, $P < 0.01$). Our results suggest that the addition of pictilisib potentiates the intracellular accumulation of DSB from clofarabine, thereby increasing cellular apoptosis.

Clofarabine and pictilisib induce DNA damage while inhibiting cell-survival signaling pathways and potentiating major regulators of apoptosis

We performed western blot analysis to validate our previous findings of increased DSB with combination treatment with clofarabine and pictilisib. In addition to measuring γ-H2AX activation, we investigated the phosphorylation of CHK2 and the cleaved fraction of PARP. CHK2 is a key component of the DNA damage response and is phosphorylated in response to DSB [39]. Consistent with our immunofluorescence findings, we found that AGS and MKN45 cells treated with clofarabine and pictilisib had increased activation of γ-H2AX, phosphorylation of CHK2, and cleaved PARP fraction compared with a single agent and vehicle control (Fig. 5A,B). This effect was seen prominently after 24 h of treatment and sustained for 48 h (Supplemental Fig. S6A,B).

We also performed western blot analysis to elucidate the effect of pictilisib on pro-survival cellular mechanisms, namely the AKT/PI3K/mTOR signaling pathway. We discovered that pictilisib inhibited AKT phosphorylation in both AGS and MKN45 cell lines. There was no discernable difference in this signaling pathway between cells treated with pictilisib alone and cells treated with both clofarabine and pictilisib (Fig. 5A,B). These effects were prominent at the 6 hour and 24-hour timepoints and dissipated after 48 h of treatment (Supplemental Fig. S6A,B). We also investigated the effects of drug treatment on the downstream mTOR target RPS6KB1. In both AGS and MKN45 cells treated with pictilisib or the combination of clofarabine and pictilisib there was decreased phosphorylation of RPS6KB1, suggesting downstream mTOR pathway inhibition (Fig. 5A,B). This effect was most pronounced at the 24-hour timepoint in both cell lines. Interestingly, single agent treatment with clofarabine resulted in increased pAKT signaling at 6 h in both AGS and MKN45 cell lines. This suggests that the addition of pictilisib to clofarabine was needed to suppress a potentially AKT-dependent resistant mechanism.

AKT is known to promote pro-survival signaling through its influence on the BCL2 family of proteins. Previous investigations have demonstrated decreased BCL2 expression with AKT inhibition [40]. Concordantly, our qRT-PCR and western blot results demonstrate significantly decreased gene and protein expression of *BCL2* in both AGS and MKN45 cell lines following treatment with pictilisib. Additionally, combined clofarabine and pictilisib treatment suppressed BCL2 expression significantly more than pictilisib alone (Fig. 5C,D, $P < 0.01$). It has been previously reported that PI3K inhibitors can upregulate several pro-apoptotic members of the BCL2 family, such as BAX and BCL2-associated agonists of cell death (BAD) [41,42]. This was again investigated with qRT-PCR and western blot. Results demonstrated significantly increased gene and protein expression of BAX and PUMA in both AGS and MKN45 cells following combined clofarabine and pictilisib treatment compared to single agent treatment or vehicle control (Fig. 5C,D, $P < 0.01$). Taken together, these results demonstrate complementary molecular actions of clofarabine and Pictilisib serve to enhance cancer cell death and suppress AKT-dependent resistant mechanisms.

The combination of clofarabine and pictilisib suppresses gastric adenocarcinoma PDX growth in vivo

To confirm our *in vitro* observations that the combination of clofarabine and pictilisib function synergistically to inhibit tumor growth, we evaluated NOD.Cg-Prkdc^{scid}/J mice implanted with 2 PDX lines. Both PDXs were generated from patients with stage IV disease, were of intestinal type, human epidermal growth factor receptor 2 (HER2) and Epstein-Barr Virus (EBV) negative. While PDX 459 was microsatellite stable and wild type for all PIK3 genes, PDX 498 demonstrated microsatellite instability and demonstrated a frameshift in PIK3C2G. Notably, *phosphatase and tensin homolog (PTEN)* and *mTOR* were wild types in both PDX samples (Supplemental Fig. S7A,B). Treatment with clofarabine 30 mg/kg as a single agent significantly inhibited tumor growth in both PDX lines compared with control tumors (Fig. 6A and D, $P < 0.01$). Combined treatment with clofarabine 30 mg/kg and pictilisib 75 mg/kg significantly inhibited tumor growth in both PDX lines compared with single agent treatment and control tumors (Fig. 6A and D, $P < 0.01$). There was no significant change in mouse weight to suggest toxicity (Fig. 6B). A subset of mice ($n = 6$ per treatment group per PDX line) reaching the conclusion of treatment duration (24 days) was then followed for survival and sacrificed once tumors reached 1000 mm^3. A Kaplan-Meier survival estimate was performed, and results demonstrated improved survival with single agent clofarabine therapy in both PDX lines compared with the control group (Fig. 6E, $P<0.01$). Survival analysis of the group receiving combined clofarabine and pictilisib therapy demonstrated significantly enhanced survival with combined therapy compared with single agent treatment or control tumors (Fig. 6E, $P < 0.01$)

We then performed western blot and immunohistochemical analysis of tumors collected after 24 days of treatment. Immunostaining with anti-Ki67 and anti-cleaved caspase-3 antibodies indicated that the slowed tumor growth in the clofarabine and combined clofarabine and pictilisib groups were likely due to decreased cellular proliferation and increased apoptosis. Ki67 immunostaining demonstrated significantly decreased staining with clofarabine treatment compared to controls and significantly increased staining with combined clofarabine and pictilisib treatment compared with all other samples (Fig. 6C, $P < 0.01$). The converse was true with cleaved caspase-3 immunostaining with significantly increased signal in the clofarabine group compared with untreated tumors and significantly increased signal with combined clofarabine and pictilisib treatment compared with all other treatment groups (Fig. 6C, $P<0.01$). Western blot analysis demonstrated increased cleaved fraction of PARP, phosphorylation of CHK2, and phosphorylation of H2AX with combined clofarabine and pictilisib treatment compared with control tumors and single agent treatment. There was also a decrease in phosphorylated AKT in tumors treated with clofarabine, pictilisib, or a combination. This decrease was most pronounced in the combination treatment group (Fig 6F).

Discussion

GC is the third most common cause of cancer-related death worldwide, causing more than 700,000 deaths each year [2,3]. Unfortunately, in the United States, most GC patients are diagnosed at a late stage (Stage III or IV) with a poor response to therapy and a five-year survival rate of 5.2% [43]. Despite significant advances in diagnostic and therapeutic modalities, GC remains a significant source of cancer-related morbidity and mortality [44]. Current treatments for GC are often met with chemoresistance and poor clinical outcomes. The AKT/PI3K/mTOR pathway is a major, frequently activated pathway in GC. It plays an integral role in chemoresistance [16,17]. Many drug-resistant tumors achieve chemoresistance through the epithelial-mesenchymal transition (EMT) and a key signaling pathway influencing EMT is AKT/PI3K [45]. Thus, this pathway is a logical source for further investigations into combinatorial efficacy with other chemotherapeutic agents.

Only recently have investigators begun to perform robust molecular profiling gastric adenocarcinoma samples and have sub-classified tumors into 4 distinct molecular subtypes [46]. While these studies have expanded our understanding of the molecular characterization of GC, they serve to highlight the intense degree of heterogeneity that exists within this specific cancer site. Thus, a standardized therapeutic regimen may not be the optimal treatment for every patient. There remains an unmet need to identify novel therapeutic options to provide greater clinical benefit on a case-by-case basis.

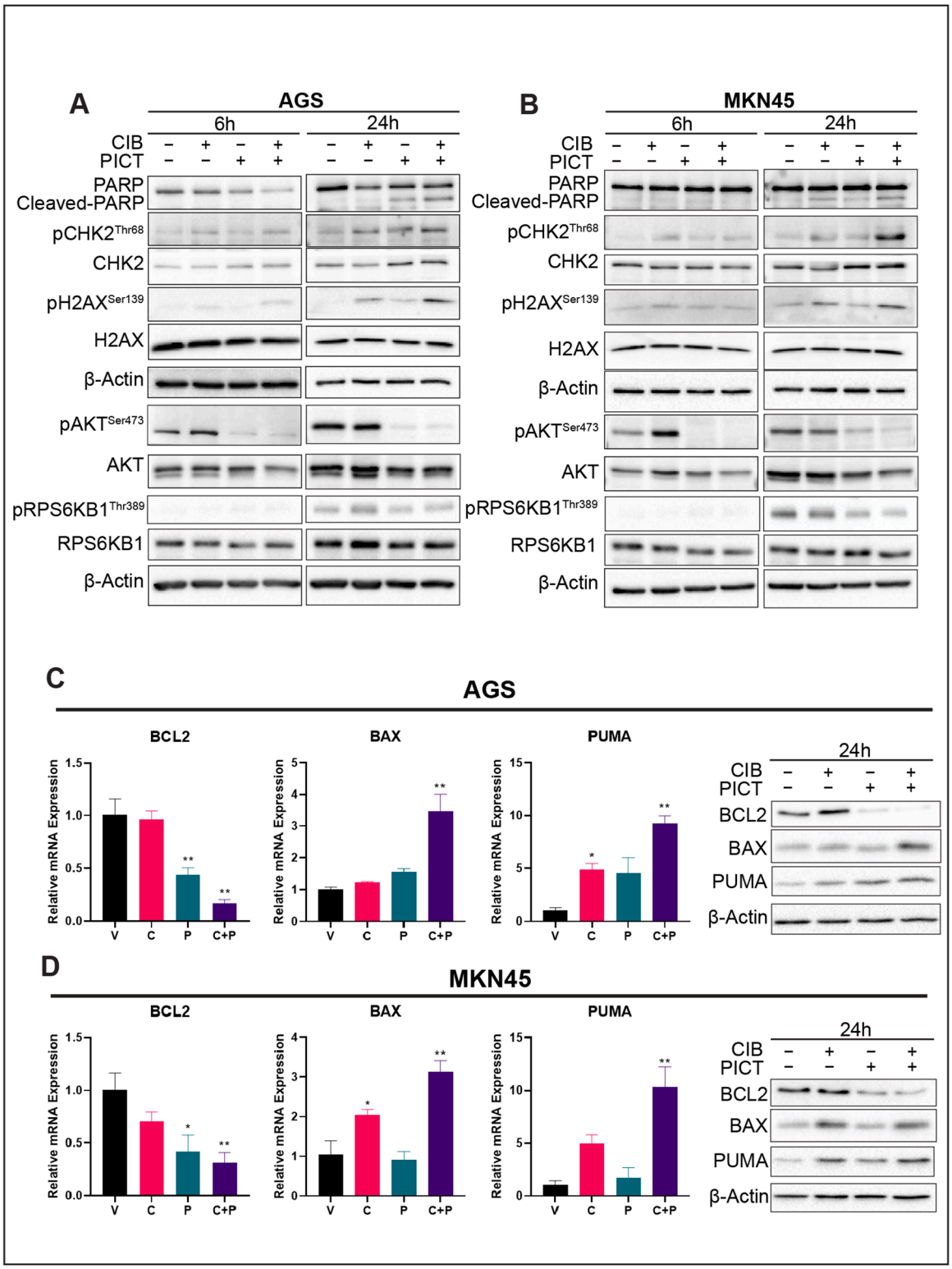

Fig. 5. Clofarabine and pictilisib combination treatment induces DNA damage and blocks cell survival signaling pathways. **A-B:** Western blot analysis for PARP/cleaved-PARP, CHK2, γ-H2AX, AKT, RPS6KB1, and β-actin following treatment with clofarabine and/or pictilisib for 6 and24 h in AGS **(A)** and MKN45 **(B)** cell lines. **C-D:** qRT-PCR and western blot analysis of BLC2, BAX, and PUMA in AGS **(C)** and MKN45 **(D)** cells treated with clofarabine and/or pictilisib for 24 h. ANOVA with Tu-Key post-hoc analysis was utilized to demonstrate statistical difference between control groups and treatment groups. Each bar in the graph represents the mean ± SD of three independent experiments. * $P < 0.05$, ** $P < 0.01$.

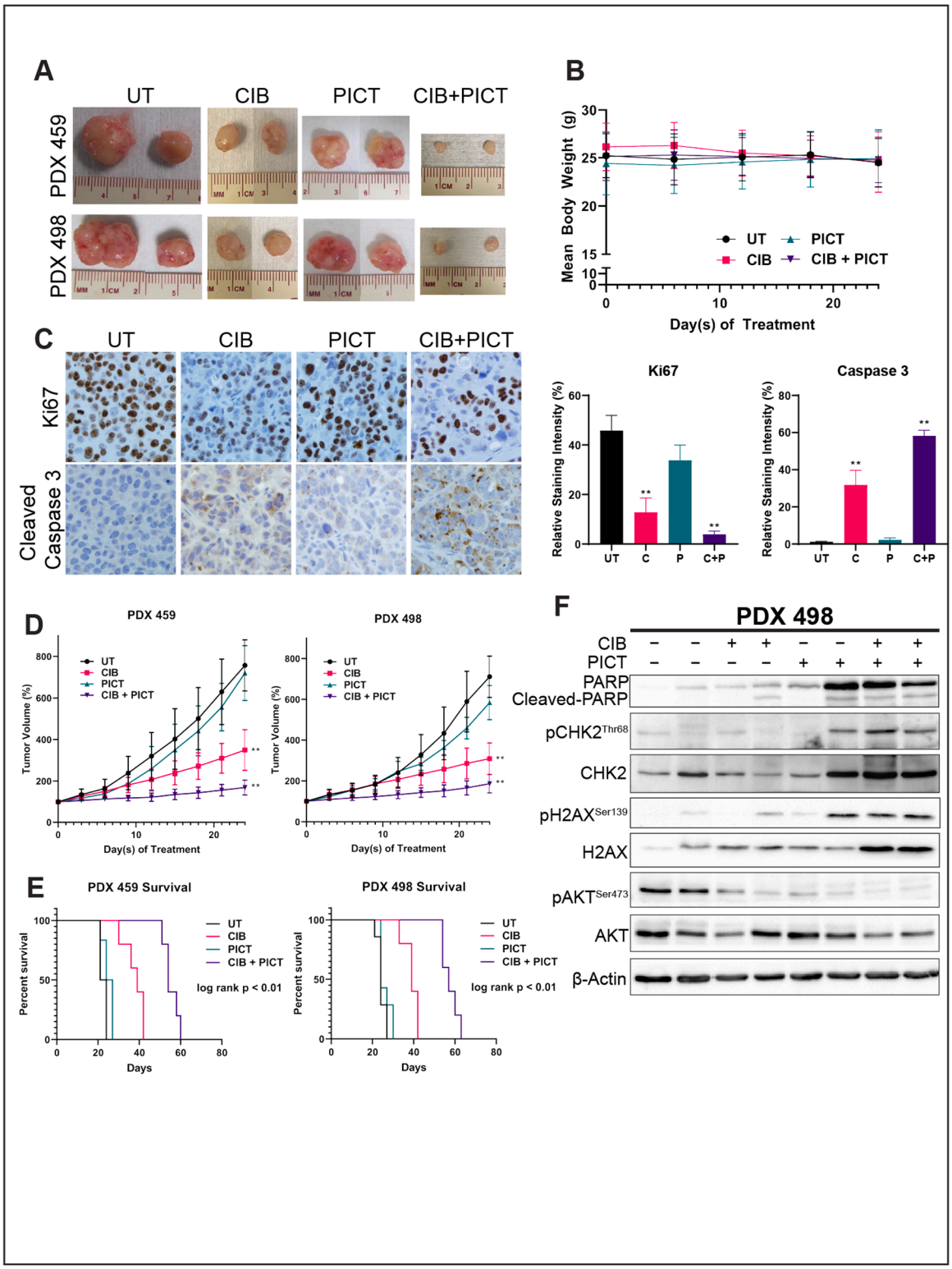

Fig. 6. Clofarabine and pictilisib combination treatment abrogates tumor growth in PDX mouse models. **A:** Representative PDX tumors of sacrificed mice at experimental endpoint of 24 days. **B:** Mean body weight (g) of PDX-implanted mice measured every 6 days for the treatment duration of 24 days. **C:** Immunohistochemistry staining for Ki67 and cleaved caspase 3 (top) and quantification of immunostaining intensity in each treatment group (bottom). **D:** Tumor volumes measured every 3 days of PDX mouse models treated with clofarabine and/or pictilisib. Each data point represents the mean ± SD of 9 PDXs. **E:** Kaplan-Meier survival estimate of 6 mice in each treatment group. **F:** Western blot analysis of PDX tumors for AKT, PARP, CHK2, H2AX, and β-actin in mice treated with clofarabine and/or pictilisib at the treatment endpoint of 24 days. A log-rank calculation was performed to demonstrate statistical significance in survival between treatment groups. One-way ANOVA with Tu-Key post-hoc analysis was utilized to demonstrate the statistical differences between control groups and treatment groups. Each bar in the graph represents the mean ± SD of three tissue sections. * $P < 0.05$, ** $P < 0.01$.

In this study, we utilize drug sensitivity screening and next generation sequencing to identify a potential therapeutic combination efficacious in pre-clinical models of GC. Our study represents the first investigation into clofarabine as a potential therapeutic agent in treating GC. DNA damaging agents/antimetabolites are considered standard of care in chemotherapeutic regimens for GC [35]. Clofarabine has a comparative advantage over these commonly used agents because it inhibits both RR and DNA polymerase. Thus, it is likely that there is a clinical role for the use of clofarabine in GC.

Clofarabine is a monotherapy that demonstrated adequate anti-tumor activity *in vitro* and *in vivo*. This effect was further enhanced with the addition of the PI3K inhibitor pictilisib. Previous investigations have demonstrated that AKT/PI3K signaling is a means of overcoming the cellular insults caused by DSB through the promotion of non-homologous end joining-mediated DSB repair and cell survival [47]. In line with this mechanism, we observed an increase pAKT when cells were treated with clofarabine as a single agent. This suggests the activation of this survival mechanism in response to DSB. Similarly, others have shown that the combination of clofarabine with the mTOR inhibitor temsirolimus has preclinical efficacy in cellular models of acute myeloid leukemia (AML) [48]. While this provides a potential explanation for the observed synergism between clofarabine and pictilisib, we acknowledge that the exact mechanism by which combination treatment achieves its enhanced anti-tumor effect will require additional investigations. Furthermore, our investigation evaluated the simultaneous administration of both drugs with favorable results. It is possible that different dose-sequence alterations may have different efficacy.

Our identification of pictilisib as a synergistic agent represents our most recent validation of the previously published SynergySeq pipeline. We have previously demonstrated that this pipeline is effective in pre-clinical models of GBM in identifying novel therapeutic combinations [10]. In this investigation, we utilized the clofarabine gene signature in AGS and MKN45 cell lines to identify compounds that would have the least similarity to clofarabine and with the highest gastric adenocarcinoma disease signature reversal. All compounds that were tested in combination with clofarabine had relatively similar orthogonality to the clofarabine signature but differed in their disease signature reversal, most notably with the ALK inhibitor NVP-TAE 684. While this compound did have some synergistic effect with clofarabine in AGS cells (CI 0.819), the synergistic effect was not as robust as pictilisib. This finding is explained by the presence of an ALK mutation in the AGS cell line, while MKN45 cells are known to be ALK wild type [49]. Oncogenic ALK mutations have been demonstrated to be present in 16% of TCGA GC samples with microsatellite instability [50]. Despite these results, the SynergySeq pipeline remains a powerful tool to predict drug efficacy in animal or human models of GC. Our findings represent an exciting opportunity for further refinement of our methodology to provide maximal clinical impact.

Numerous PI3K inhibitors have been approved by the FDA for treatment of hematological malignancies. While these agents have significant therapeutic benefits, there is some concern regarding the sometimes severe adverse effects associated with their use [51]. Other *in vivo* investigations of pictilisib have shown that doses of up to 150 mg/kg/day can be safely tolerated [52]. In our investigation, we elected to limit the dosing of pictilisib to 75 mg/kg/day to minimize the risk of toxicity. We were still able to demonstrate significantly decreased tumor growth at lower doses of pictilisib without significant weight changes to suggest drug toxicity (Supplemental Fig. 7). This highlights the great advantage to the administration of synergistic agents: enhanced anti-tumorigenic effects at lower doses.

In conclusion, our results validate a potentially transformative pipeline in individualized care for patients with GC. We demonstrate that the novel combination of clofarabine and pictilisib promotes DNA damage and inhibits key cell survival pathways to induce cell death beyond single-agent treatment. Our results provide a proof-of-concept for synergistic activity between DNA damaging agents and PI3K inhibitors in GC. While some limitations still exist, we envision that the workflow could be the future for targeted cancer therapeutics. As the cost of performing next-generation sequencing continues to decline, the possibility of patient-specific therapeutic becomes an ever-closer reality.

Funding

This study was supported by grants from the U.S. National Institutes of Health (R01CA249949, T32 CA211034, and LINCS-DCIC U54HL127624), National Cancer Institute (P30CA240139), and the U. S. Department of Veterans Affairs (1IK6BX003787 and I01BX001179). The use of the Molecular Therapeutics Shared Resource (MTSR) and Flow Cytometry Shared Resource (FCSR) was supported by the Sylvester Comprehensive Cancer Center Support Grant (P30CA240139). This work's content is solely the responsibility of the authors. It does not necessarily represent the official views of the Department of Veterans Affairs, National Institutes of Health, National Cancer Institute, or the University of Miami.

Data availability

The raw read data from our mRNA sequencing reported in this paper have been deposited in the GEO data repository (GSE174288).

Declaration of Competing Interest

The authors declare that they have no known competing financial interests or personal relationships that could have appeared to influence the work reported in this paper.

Supplementary materials

Supplementary material associated with this article can be found, in the online version, at doi:10.1016/j.tranon.2021.101260.

References

[1] P. Bertuccio, et al., Recent patterns in gastric cancer: a global overview, Int. J. Cancer 125 (3) (2009) 666–673.
[2] F. Bray, et al., Global cancer statistics 2018: GLOBOCAN estimates of incidence and mortality worldwide for 36 cancers in 185 countries, CA Cancer J. Clin. 68 (6) (2018) 394–424.
[3] R.L. Siegel, K.D. Miller, A. Jemal, Cancer statistics, 2020, CA Cancer J. Clin. 70 (1) (2020) 7–30.
[4] Mansfield, P.F., Clinical features, diagnosis, and staging of gastric cancer. *UpToDate.* K. Tanabe, et al., Editors. (2021). Accessed June 14, 2020 from https://www.uptodate.com/contents/clinical-features-diagnosis-and-staging-of-gastric-cancer.
[5] J.J. Marin, et al., Mechanisms of resistance to chemotherapy in gastric cancer, Anticancer Agents Med. Chem. 16 (3) (2016) 318–334.
[6] R.T. Swords, et al., Ex-vivo sensitivity profiling to guide clinical decision making in acute myeloid leukemia: a pilot study, Leuk. Res. 64 (2018) 34–41.
[7] I. Lohse, et al., Ex vivo drug sensitivity testing as a means for drug repurposing in esophageal adenocarcinoma, PLoS One 13 (9) (2018), e0203173.
[8] I. Lohse, et al., Ovarian cancer treatment stratification using ex vivo drug sensitivity testing, Anticancer Res. 39 (8) (2019) 4023–4030.
[9] D. Essegian, et al., The clinical kinase index: a method to prioritize understudied kinases as drug targets for the treatment of cancer, Cell Rep. Med. 1 (7) (2020), 100128.
[10] V. Stathias, et al., Drug and disease signature integration identifies synergistic combinations in glioblastoma, Nat. Commun. 9 (1) (2018) 5315.
[11] AdisInsight, Clofarabine, Drugs R. D. 5 (4) (2004) 213–217, https://doi.org/10.2165/00126839-200405040-00005.
[12] A. Zhenchuk, et al., Mechanisms of anti-cancer action and pharmacology of clofarabine, Biochem. Pharmacol. 78 (11) (2009) 1351–1359.
[13] N. Hijiya, et al., Phase 2 trial of clofarabine in combination with etoposide and cyclophosphamide in pediatric patients with refractory or relapsed acute lymphoblastic leukemia, Blood 118 (23) (2011) 6043–6049.
[14] X. Wang, F. Albertioni, Effect of clofarabine on apoptosis and DNA synthesis in human epithelial colon cancer cells, Nucleosides Nucleotides Nucl. Acids 29 (4–6) (2010) 414–418.
[15] T. Takahashi, et al., Antitumor activity of 2-chloro-9-(2-deoxy-2-fluoro-beta-D-arabinofuranosyl) adenine, a novel deoxyadenosine analog, against human colon tumor xenografts by oral administration, Cancer Chemother. Pharmacol. 43 (3) (1999) 233–240.

[16] B. Ye, et al., Expression of PI3K/AKT pathway in gastric cancer and its blockade suppresses tumor growth and metastasis, Int. J. Immunopathol. Pharmacol. 25 (3) (2012) 627–636.
[17] H.G. Yu, et al., Phosphoinositide 3-kinase/Akt pathway plays an important role in chemoresistance of gastric cancer cells against etoposide and doxorubicin induced cell death, Int. J. Cancer 122 (2) (2008) 433–443.
[18] N. Yamamoto, et al., Phase Ia/Ib study of the pan-class I PI3K inhibitor pictilisib (GDC-0941) administered as a single agent in Japanese patients with solid tumors and in combination in Japanese patients with non-squamous non-small cell lung cancer, Invest. New Drugs 35 (1) (2017) 37–46.
[19] D. Sarker, et al., First-in-human phase I study of pictilisib (GDC-0941), a potent pan-class I phosphatidylinositol-3-kinase (PI3K) inhibitor, in patients with advanced solid tumors, Clin. Cancer Res. 21 (1) (2015) 77–86.
[20] K. Ishida, et al., Inhibition of PI3K suppresses propagation of drug-tolerant cancer cell subpopulations enriched by 5-fluorouracil, Sci. Rep. 7 (1) (2017) 2262.
[21] S. Leong, et al., A phase i dose-escalation study of the safety and pharmacokinetics of pictilisib in combination with erlotinib in patients with advanced solid tumors, Oncologist 22 (12) (2017) 1491–1499.
[22] A. Dobin, et al., STAR: ultrafast universal RNA-seq aligner, Bioinformatics 29 (1) (2013) 15–21.
[23] M.I. Love, W. Huber, S. Anders, Moderated estimation of fold change and dispersion for RNA-seq data with DESeq2, Genome Biol. 15 (12) (2014) 550.
[24] G. Yu, et al., clusterProfiler: an R package for comparing biological themes among gene clusters, OMICS 16 (5) (2012) 284–287.
[25] Carlson M. (2019). *org.Hs.eg.db: Genome wide annotation for Human.* R package version 3.8.2. Accessed May 12, 2020 from https://bioconductor.org/packages/release/data/annotation/html/org.Hs.eg.db.html, doi:10.18129/B9.bioc.org.Hs.eg.db.
[26] Y. Benjamini, Y. Hochberg, Controlling the false discovery rate: a practical and powerful approach to multiple testing, J. R. Stat. Soc. Ser. B (Methodological) 57 (1) (1995) 289–300.
[27] M. Kanehisa, S. Goto, KEGG: kyoto encyclopedia of genes and genomes, Nucl. Acids Res. 28 (1) (2000) 27–30.
[28] A. Subramanian, et al., A next generation connectivity map: L1000 platform and the first 1,000,000 Profiles, Cell 171 (6) (2017) 1437–1452, e17.
[29] L. Collado-Torres, et al., Reproducible RNA-seq analysis using recount2, Nat. Biotechnol. 35 (4) (2017) 319–321.
[30] A. Colaprico, et al., TCGAbiolinks: an R/Bioconductor package for integrative analysis of TCGA data, Nucl. Acids Res. 44 (8) (2016) e71.
[31] T.C. Chou, Drug combination studies and their synergy quantification using the Chou-Talalay method, Cancer Res. 70 (2) (2010) 440–446.
[32] K.J. Livak, T.D. Schmittgen, Analysis of relative gene expression data using real-time quantitative PCR and the 2(-Delta Delta C(T)) Method, Methods 25 (4) (2001) 402–408.
[33] A.R. Crowe, W. Yue, Semi-quantitative determination of protein expression using immunohistochemistry staining and analysis: an integrated protocol, Bio Protoc. 9 (24) (2019).
[34] S. Corso, et al., A comprehensive PDX gastric cancer collection captures cancer cell-intrinsic transcriptional MSI traits, Cancer Res. 79 (22) (2019) 5884–5896.
[35] S.D. Kamath, A. Kalyan, A.B. Benson 3rd, Pembrolizumab for the treatment of gastric cancer, Expert Rev. Anticancer Ther. 18 (12) (2018) 1177–1187.
[36] H. Ghanem, et al., Clofarabine in leukemia, Exp. Rev. Hematol. 3 (1) (2010) 15–22.
[37] A. Sharma, K. Singh, A. Almasan, Histone H2AX phosphorylation: a marker for DNA damage, Methods Mol. Biol. 920 (2012) 613–626.
[38] L.C. Crowley, et al., Quantitation of apoptosis and necrosis by annexin v binding, propidium iodide uptake, and flow cytometry, Cold Spring Harb. Protoc. 2016 (11) (2016).
[39] L. Zannini, D. Delia, G. Buscemi, CHK2 kinase in the DNA damage response and beyond, J. Mol. Cell Biol. 6 (6) (2014) 442–457.
[40] S. Pugazhenthi, et al., Akt/protein kinase B up-regulates Bcl-2 expression through cAMP-response element-binding protein, J. Biol. Chem. 275 (15) (2000) 10761–10766.
[41] P. Bose, M. Rahmani, S. Grant, Coordinate PI3K pathway and Bcl-2 family disruption in AML, Oncotarget 3 (12) (2012) 1499–1500.
[42] S.R. Datta, et al., Akt phosphorylation of BAD couples survival signals to the cell-intrinsic death machinery, Cell 91 (2) (1997) 231–241.
[43] A.M. Noone, et al., Cancer incidence and survival trends by subtype using data from the surveillance epidemiology and end results program, 1992-2013, Cancer Epidemiol. Biomark. Prev. 26 (4) (2017) 632–641.
[44] Collaborators, G.B.D.S.C., The global, regional, and national burden of stomach cancer in 195 countries, 1990-2017: a systematic analysis for the Global Burden of Disease study 2017, Lancet Gastroenterol. Hepatol. 5 (1) (2020) 42–54.
[45] W. Xu, Z. Yang, N. Lu, A new role for the PI3K/Akt signaling pathway in the epithelial-mesenchymal transition, Cell Adh. Migr. 9 (4) (2015) 317–324.
[46] Cancer Genome Atlas Research, N., Comprehensive molecular characterization of gastric adenocarcinoma, Nature 513 (7517) (2014) 202–209.
[47] M. Fraser, et al., MRE11 promotes AKT phosphorylation in direct response to DNA double-strand breaks, Cell Cycle 10 (13) (2011) 2218–2232.
[48] F. Chiarini, et al., A combination of temsirolimus, an allosteric mTOR inhibitor, with clofarabine as a new therapeutic option for patients with acute myeloid leukemia, Oncotarget 3 (12) (2012) 1615–1628.
[49] J.G. Tate, et al., COSMIC: the catalogue of somatic mutations in cancer, Nucleic Acids Res. 47 (D1) (2018) D941–D947.
[50] B.W. Katona, A.K. Rustgi, Gastric cancer genomics: advances and future directions, Cell Mol. Gastroenterol. Hepatol. 3 (2) (2017) 211–217.
[51] I.B. Greenwell, A. Ip, J.B. Cohen, PI3K Inhibitors: understanding Toxicity Mechanisms and Management, Oncology (Williston Park) 31 (11) (2017) 821–828.
[52] J.J. Wallin, et al., GDC-0941, a novel class I selective PI3K inhibitor, enhances the efficacy of docetaxel in human breast cancer models by increasing cell death in vitro and in vivo, Clin. Cancer Res. 18 (14) (2012) 3901–3911.